

Direct Solvent-Free Amide Bond Formation Catalyzed by Anatase-TiO₂ Surface: Insight from Modeling

Ettore Fois and Gloria Tabacchi*

Amide bond formation processes are of paramount relevance for a broad spectrum of applications. Conventional amidation protocols typically rely on drastic reaction conditions and the use/disposal of large amounts of chemicals. These limitations may be bypassed by heterogeneously catalyzed amidation at dry conditions. However, progress is hindered because the mechanisms of these processes are largely unexplored. By using *ab initio* metadynamics, a concerted one-step mechanism is proposed for the solvent-free condensation of methylamine and formic acid on TiO₂(101)-anatase, leading to methylformamide with concomitant release of molecular water. The activation barrier—14.3 kcal mol⁻¹—is in line with the mild conditions experimentally adopted in amide bond syntheses on TiO₂ nanoparticles. The mechanism disclosed herein reveals the key role of Ti⁴⁺ sites located on stoichiometric (101) anatase surfaces in promoting amide-bond formation at the TiO₂/vapor interface. The acid strength of the adsorbed HCOOH molecules may be tuned by the HCOOH surface coverage, thus influencing the outcome of the amidation reaction. These molecular-level insights may foster further endeavors to improve/upscale TiO₂-catalyzed amide syntheses at dry conditions, while raising the interest toward amidation processes at the surface/vapor interface promoted by economically and environmentally sustainable metal oxide nanomaterials.

1. Introduction

Amide linkages are ubiquitous in chemical products covering a wide spectrum of applications—ranging from high-performance polymer materials such as polyamides and polyimides to agrochemistry, cosmetics, and pharmaceutical industry.^[1] Amides can be formally synthesized from condensation reactions between amines and carboxylic acids, producing water as a byproduct. Yet, the nucleophilic attack of the amine on the carboxyl moiety normally requires drastic temperature conditions (higher than 140 °C), leading to unwanted side processes—such


as, e.g., salt formation between carboxylic acids and amines—and, consequently, to waste byproducts which must be eliminated from the reaction system.^[2,3] Although the use of catalysts can increase the electrophilic character of the carboxyl group—thus favoring amine attack over deprotonation—the amidation process still requires considerable reaction times, inert atmospheres, and elevated temperatures.^[4] Moreover, since water molecules are produced in the condensation reaction, toxic, polluting, and/or hazardous solvents like benzene, toluene, or tetrahydrofuran are needed to eliminate H₂O from the reaction mixture via azeotropic distillation.^[5] Therefore, in the quest for a more sustainable development, “rethinking amide bond synthesis” still remains a key challenge in chemistry.^[1]

Several amidation reactions have been proposed over the last decades to try to overcome synthetic issues while guaranteeing large-scale production standards.^[1,2,6] These issues are generally dealt with by implementing indirect condensation processes, in which preactivated derivatives

of carboxylic acids are used. However, conventional routes to amide bond formation—although successful—are plagued by a common “poor atom economy” issue, i.e., the use of large amounts of chemicals—mostly coupling reagents and organic solvents.^[6] Additionally, the purification of the amide molecules and the secure disposal of solvents and by-products pose crucial challenges to sustainability. The issues of waste and expense associated with amidation are responsible, for example, of the soaring cost of therapeutic peptides, along with the energetic costs and environmental risks associated with the elimination of byproducts. Indeed, already back in 2007, the ACS Green Chemistry Institute Pharmaceutical Roundtable voted “amide bond formation avoiding poor atom economy reagents”^[4] as a top priority in the search for better and greener reagents and methods. The list was revised in 2018, and “*General methods for catalytic/sustainable (direct) amide or peptide formation*” is still one of the “Key Green Chemistry Research Areas” selected by the Roundtable.^[7] Indeed, although much effort has been devoted toward the development of greener amidation protocols,^[6] this issue still remains open.

In the quest of sustainability, amide-bond formation processes promoted by heterogeneous catalysts could be advantageous over homogeneously catalyzed ones, due to their inherent ease of catalysts’ separation and recycling, especially by keeping in mind

E. Fois, G. Tabacchi
Dipartimento di Scienza e Alta Tecnologia and INSTM
Università degli Studi dell’Insubria
via Valleggio 11, I-22100 Como, Italy
E-mail: gloria.tabacchi@uninsubria.it

 The ORCID identification number(s) for the author(s) of this article can be found under <https://doi.org/10.1002/ssr.202400346>.

© 2024 The Author(s). Small Structures published by Wiley-VCH GmbH. This is an open access article under the terms of the Creative Commons Attribution License, which permits use, distribution and reproduction in any medium, provided the original work is properly cited.

DOI: 10.1002/ssr.202400346

the long times and poor-atom-economy processes required for the recovery of homogeneous catalysts from liquid reaction mixtures.^[5] In this respect, several catalysts have been successfully tested, including, e.g., clays,^[8] zeolites,^[9] mesoporous silicas,^[10] metal oxides,^[3] and metal–organic frameworks.^[11,12] Nonetheless, amidation processes relying on heterogeneous catalysis would be maximally beneficial if the carboxylic group could be activated toward amine attack directly by a solid catalyst and without the waste-intensive use of potentially dangerous organic solvents. Notably, in direct solvent-free conditions, water would be the only condensation byproduct, thus making such procedures for amide bond formation a key step toward a sustainable future. Despite several endeavors—based on the use of graphene oxide,^[13] and metal oxide nanosystems^[14,15] as heterogeneous catalysts—such an appealing route has not been thoroughly pursued yet. This is partly due to the fact that, to become competitive with traditional protocols relying on solvents and coupling agents, important challenges still remain to be met, such as the achievement of high yielding at low temperatures and mild conditions, a broad reaction scope and the ability to function efficiently with a variety of substrates.^[6]

A primary key ingredient needed to meet these challenges is molecular-level insight on the mechanism of known solvent-free direct amidation processes based on solid catalysts. For example, a detailed microscopic knowledge of the structure of the activated complex would greatly help the design of new and more efficient heterogeneous catalysts, and the subsequent optimization of the reaction conditions. In this context, relevant theoretical insight has been achieved on peptide bond formation, namely, the condensation of simple aminoacids catalyzed by TiO₂,^[16] and even on the amidation process on amorphous silica,^[17] both at dry conditions. In the first case, it has been found that the peptide bond formation proceeds via a two-step mechanism, involving first the nucleophilic attack and proton transfer by a gas-phase aminoacid molecule to a second aminoacid molecule dissociatively adsorbed on TiO₂, and then the transfer of a surface proton to the aminoacid hydroxyl group.^[16] As regards amide bond formation on amorphous silica, surface silanols pairs separated by ≈5 Å have been identified as the key active sites, because they can accommodate in a suitable orientation coexisting pairs of amine/carboxylic acid reactants in their neutral and in their zwitterionic forms. The amidation of the neutral amine/carboxylic acid pair is promoted by the zwitterionic pair, which plays a vital role in the formation of the water molecule, thus acting as the actual catalyst for the dehydration step of the process.^[17]

Among the heterogeneous catalysts used in reported direct solvent-free amide bond formation, titanium dioxide (nano) materials have shown to be excellent candidates, owing to their environmentally benign nature joint to their high catalytic activity, selectivity, and reusability.^[18] Although titania has been already successfully employed as a direct amidation catalyst—, e.g., in the form of nanotubes,^[18] nanoparticles,^[18,19] nanosized sulfated titania,^[15] the understanding of the solvent-free TiO₂-catalyzed amide bond formation mechanism has yet to be accomplished.

Infrared (IR) spectroscopy provided evidence of the direct amidation of carboxylate species at the gas/titania nanoparticles interface. Specifically, by dosing simple carboxylic acids (formic or acetic acid) in the vapor-phase on the surface of dehydrated

and stoichiometric TiO₂-P25 nanoparticles, and then adding 1-pentanamine vapor, characteristic IR bands belonging to a newly formed amide species were observed.^[19] An increase of the electrophilic character of the carboxylate C atom was hypothesized, caused by the binding of the carboxylate oxygens with surface Ti⁴⁺ sites, characterized by well-known Lewis acid properties. As a result, the direct nucleophilic attack by the nitrogen atom of the amine became feasible at mild temperature conditions (about 50 °C).^[19] However, IR data did not provide hints on the reaction mechanism. First, the question as to whether the adsorbed HCOOH moiety is attacked by the vapor-phase amine, or rather the reaction occurs between chemisorbed species, still remains open. Also, although in principle one cannot exclude a role of low-concentration defects and/or different TiO₂ phases in the amidation process, from a fundamental viewpoint it is important to establish whether such a direct solvent-free amidation, could occur even in the absence of hydroxyl groups or other types of surface defects like oxygen vacancies,^[20,21] namely, on a defect-free TiO₂ surface as hypothesized in ref. [19]. Indeed, defect-free stoichiometric (101) TiO₂ anatase can catalyze a similar process, i.e., solvent-free peptide condensation.^[16,22,23]

A further open issue is how the only by-product of the reaction—water—emerges from the condensation process. Indeed, spectroscopic data did not allow one to establish if water is generated as chemisorbed (H⁺) + (OH⁻) species, physisorbed H₂O, or vapor-phase H₂O.^[19] Finally, an estimate of the activation barrier joint to a knowledge of the transition state (TS) features would be of key relevance in the endeavor to improve the reaction rate, to scale the process, and to extend it to other substrates.

The absorption of small carboxylic acids on titania surface has been intensively studied, both experimentally and by modeling.^[24–42] Overall, a widely accepted picture is that the unprotonated oxygen of the carboxyl group is linked to a surface Ti, which acts as a Lewis acid, while the hydroxyl group is directed toward a neighboring surface oxygen.^[24–28,30,31,33,36,37,42]

In a previous study, we proposed that the adsorption of carboxylic acids on anatase TiO₂(101) leads to the formation of a short-strong hydrogen bond (SSHB) with covalent character between the carboxyl proton and a surface oxygen. Such an interaction is governed either by rapid molecule-surface proton shuttling (at room temperatures) or by proton sharing due to quantum delocalization effects (at low temperatures).^[43] In both cases, the adsorbed carboxylic acid might be considered as a pre-reactant, whose Brønsted-acid functionality is both damped and protected by the anatase surface, thus allowing—in principle—for its condensation with an incoming amine molecule, while inhibiting, at the same time, parasite processes like salt formation reactions which generally burden conventional amidation protocols.

By using a modeling approach based on density functional theory (DFT), ab initio molecular dynamics (AIMD),^[44,45] and ab initio metadynamics,^[46,47] here we show that gas-phase methylamine directly attacks the carbonyl group of TiO₂-adsorbed formic acid in an Eley–Rideal fashion, producing adsorbed methylformamide and liberating a gas-phase water molecule equivalent. Such a direct amidation process can occur on defect-free anatase TiO₂(101) surface, and does not rely on the presence of peculiar surface defects (e.g., –OH groups or oxygen vacancies). In contrast, we show that HCOOH coadsorbed

species can play an indirect but fundamental role in the amidation process. After the formation of an adduct, involving a strong interaction between methylamine N atom and the C atom of adsorbed formic acid, the actual condensation occurs, affording the products with an energy barrier— 60 kJ mol^{-1} ($14.3 \text{ kcal mol}^{-1}$)—compatible with the mild reaction conditions experimentally adopted.

Although we do not rule out a possible role of minority sites (on, e.g., rutile or other anatase facets) or surface defects in this process, the picture proposed here sheds more light on the role of standard Ti sites exposed on (101) anatase surfaces—the most common terminations of commercial TiO_2 nanoparticles—in solvent-free amide-bond formation processes, and might help to upgrade TiO_2 -catalyzed amidation through a knowledge-based approach.

2. Results and Discussion

The building of the simulation system required a careful consideration of the experimental conditions at which the solvent-free TiO_2 -catalyzed amidation was conducted. The actual experiment employed commercial TiO_2 -P25 nanoparticles—exposing primarily anatase (101) facets,^[48] which were subjected to a preliminary high-temperature treatment aimed at removing all physisorbed and chemisorbed water molecules from the surface terminations. Then, exposure to molecular O_2 at 723 K was carried out to fully eliminate oxygen vacancies generated in the dehydroxylation-dehydration process. At the end of these pre-treating procedures, the catalyst was constituted by stoichiometric TiO_2 .^[19] Moreover, due to the scarce proportion of surface $-\text{OH}$ defects left on the dehydrated nanoparticles, the catalytic role of TiO_2 in the amidation was primarily ascribed to standard Ti^{4+} and O^{2-} surface sites on regular anatase (101), rather than to a limited number of defects located, e.g., on edges and corners of the nanoparticles.^[19] This argument is also corroborated by experiments on peptide bond formation on regular anatase- TiO_2 nanoparticles, indicating that aminoacids' condensation does not need peculiar defects, or highly energetic and

uncommon surface terminations, but it takes place on the stoichiometric, most stable and abundant anatase (101) facets.^[22] Hence, we focused on stoichiometric nondefective anatase $\text{TiO}_2(101)$, and modeled the adsorption of formic acid on this surface.

2.1. Results with Minimal HCOOH Coverage

A first investigation was performed on a model constituted by an anatase $\text{TiO}_2(101)$ slab featuring one adsorbed HCOOH molecule, and a gas phase methylamine molecule ($\text{HCOOH@TiO}_2(101) + \text{CH}_3\text{NH}_2$, see also Section S3, Supporting Information). Such a system, denoted Model 0, is graphically represented in **Figure 1a**.

An exploratory free energy landscape study, aimed at the simulation of the solvent-free amide formation on this system, was carried out via the Bluemoon Ensemble (BM) approach,^[49,50] by adopting the C1–N1 distance as reaction coordinate r . The resulting free energy profile is reported in Figure S2 (see also paragraph S3.1, Supporting Information).

The free energy profile shows that the decrease of the C–N distance is accompanied by a free energy rise, reaching a barrier of $10.6 \text{ kcal mol}^{-1}$ at $r = 1.8 \text{ \AA}$ —which may be considered a TS, featuring the incipient formation of a $\text{CH}_3\text{NH}_2\text{--HCOOH}$ adduct (Figure 1b), and then smoothly decreasing up to a very shallow relative minimum, located at $r = 1.68 \text{ \AA}$ (Figure 1c). Such a minimum corresponds to a very strong adduct between methylamine and the adsorbed HCOOH molecule. This moiety is characterized by a tetra-coordinated N1 atom and it is bound to a surface Ti atom through the carbonyl oxygen O1' (see Figure 1c). However, a further decrease of the reaction coordinate leads to a sharp rise of the free energy for $r < 1.5 \text{ \AA}$. The absence of further minima in the free energy profile indicates that the amidation reaction has not reached completion. This finding did suggest that a single “reaction coordinate” (the C1–N1 distance) was not sufficient to accomplish the amidation process (see also Movie S1, Supporting Information).

We decided therefore to add a second “reaction coordinate” related to both the cleavage of an N1–H bond and the formation

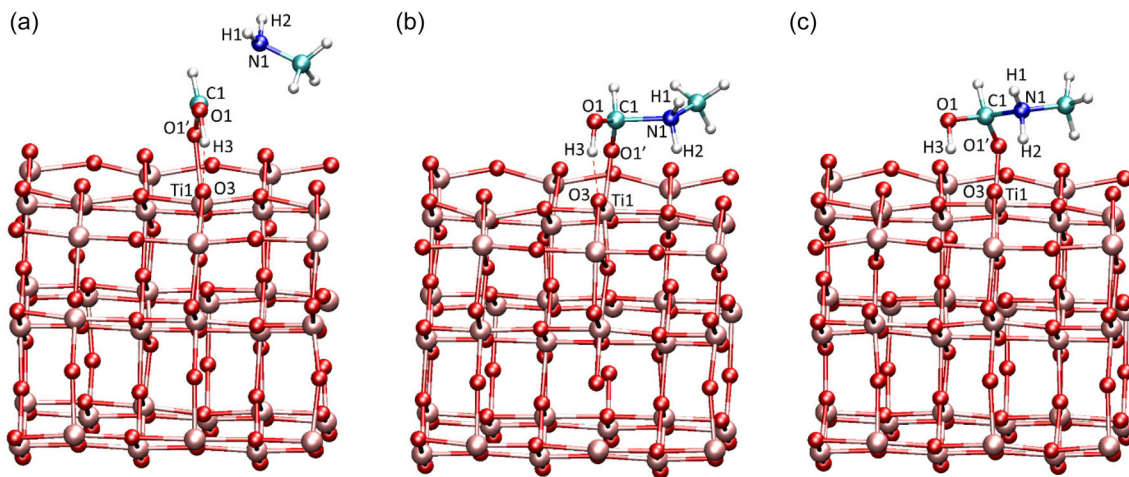


Figure 1. Graphical representations of Model 0: a) starting configuration for the BM simulations; b) TS; and c) relative free-energy minimum featuring the $\text{CH}_3\text{NH}_2\text{--HCOOH}$ adduct. Color codes: pink = Ti; red = O; blue = N; cyan = C; white = H. Red dashed lines represent hydrogen bonds.

of a new O1–H bond. As metadynamics is a more efficient approach for treating simultaneously more than one reaction coordinates (denoted collective variables, CVs), we shifted to this approach. The first collective variable CV1 was the same as in the BM simulations (the C1–N1 distance). For the second collective variable CV2, we chose the difference between the H1–N1 distance and the H1–O1 distance. The results of this metadynamics simulation are reported in paragraph S3.2 and sketched in Movie S2, Supporting Information. Also in this simulation, the amidation process was not accomplished: indeed, the C1–N1 and the H1–O1 distances remained too large to allow for the formation of an amide bond (see Figure S4, Supporting Information).

Therefore, to gain further guidance in the selection of alternative CVs, we performed a standard equilibrium AIMD simulation on Model 0 (see also paragraph S3.3, Supporting Information). Importantly, migration of the hydroxyl proton toward the amine was observed after a few ps simulation, leading to the formation of HCOO[−] and CH₃NH₃⁺ (see Movie S3 and Figure S5, Supporting Information). Hence, this simulation spontaneously led to the parasite salt-formation process, which is experimentally a well-known limitation of direct amidation routes.^[2,3] The fact that such an event has been observed during a standard AIMD simulation indicates that, if only one molecule of formic acid is adsorbed on the model slab, the salt-formation reaction may easily occur at $T = 320$ K. On this basis, Model 0, exhibiting a minimal HCOOH coverage of the TiO₂(101) slab, was discarded, and attention was focused on a new model, built by doubling the HCOOH coverage with respect to Model 0.

2.2. Results with Higher HCOOH Coverage

The final model system for studying the amidation reaction was built by positioning two formic acid molecules on top of two Ti surface sites separated by 5.590 Å. Such a configuration resulted from geometry optimizations pertaining to different relative positioning of the two HCOOH on the model slab (see Figure S6 and paragraph S4.1, Supporting Information). Since, in the experiment, gas phase amine is introduced on the already partially HCOOH-covered catalyst's surface, a methylamine was placed at 5 Å from the surface, equally separated from the C atoms of the two adsorbed HCOOH. With such a starting configuration, the system was equilibrated at 320 K with equilibrium AIMD (see paragraph S4.2, Supporting Information). Remarkably, no hints of the salt-formation reaction were detected along the trajectory, as can be seen in Movie S4. Indeed, both the hydroxyl protons remain located between the HCOOH molecules and the surface oxygens for the whole trajectory, while the amine N1 atom approaches the C1 atom of one of the two adsorbed HCOOH. Altogether, these findings suggested that this degree of HCOOH coverage (2 acid molecules per simulation cell) could be a good choice as a starting point to perform a full study of the amidation reaction.

The choice of the collective variables (CVs) is a critical preliminary step for a successful metadynamics simulation, because the selection should include all the key microscopic variables describing the chemical transformation under study—for example, variations in specific interatomic distances or atomic coordination numbers. Although metadynamics does not

provide ready-to-use criteria to guide the CV's selection, some hints may be gathered from the dynamical behavior of the model system in the AIMD simulation (Movie S4). Overall, while the HCOOH molecules stayed steadily adsorbed on the surface, methylamine always remained in the gas-phase while approaching one of the adsorbed carboxylic acid molecules. The final configuration obtained from the equilibration run is shown in **Figure 2**. Both formic acid molecules are bound to the surface with their carbonyl oxygens coordinated to Ti sites, and with their hydroxyl groups forming SSBH with surface oxygen atoms. Remarkably, the methylamine molecule is pointing its –NH₂ group toward the C atom of one of the adsorbed formic acid moieties (C1), with the nitrogen (N1) and carbon (C1) atoms separated by a 2.794 Å distance (see Figure 2). This result suggested that the final configuration of the AIMD equilibration run could be a good starting point for the metadynamics simulation. Even more importantly, the dynamic evolution of the system confirmed that the N1–C1 interatomic separation might be a plausible choice as a CV (CV1) for the condensation process, especially keeping into account that an N–C covalent bond must form in the reaction.

In Model 0, the choice of the difference between the N1–H1 and O1–H1 distances as CV2 did not lead to a reactive path. The reason may be due to the fact that both CV1 and CV2 depend on

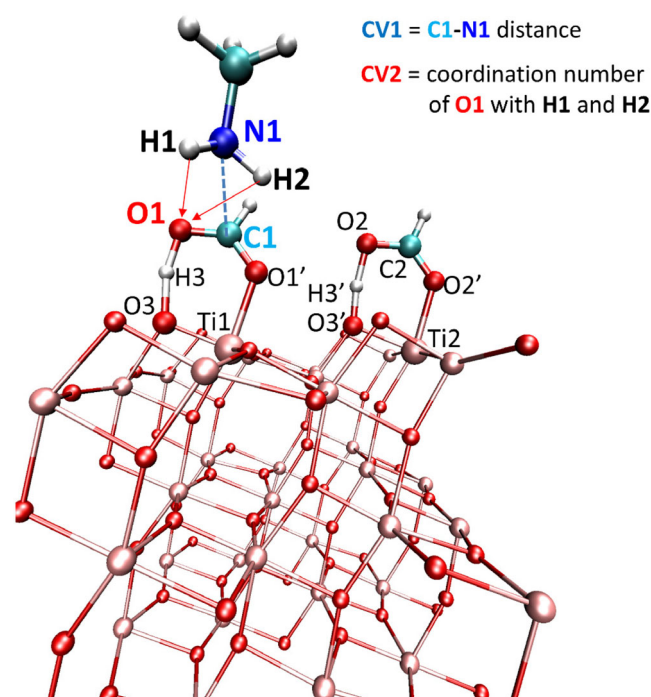


Figure 2. Graphical representation of the final configuration of the equilibration AIMD simulation, showing the content of the simulation cell adopted in the final model. Two formic acid molecules are adsorbed on top of the TiO₂(101) slab, while a methylamine molecule is present in the gas phase. The collective variables selected for metadynamics are the N1–C1 distance (CV1, represented as a blue dashed line) and the coordination number of the O1 hydroxyl oxygen with the H1 and H2 protons (CV2, represented by red solid arrows). Labels referring to the atoms involved in the CVs are highlighted in bold. Color codes: pink = Ti; red = O; blue = N; cyan = C; white = H.

the N1 atom, and probably they do not completely fulfill the CVs orthogonality conditions, which would be optimal for a successful metadynamics simulation^[47,51,52] (see also S1.4 and S3.2, Supporting Information). Thus, one needs to look for a different selection of the CV2.

A direct amidation at the TiO₂/gas interface would also imply the breakage of a C–O bond of the adsorbed carboxylic acid, and the liberation of a formal H₂O equivalent—either as molecular water, or as H⁺ + OH[−] moieties chemisorbed on the surface. In both cases, the coordination number of the O atom leaving the carboxylate moiety should increase along the amidation process. For this reason, we selected as second CV (CV2) the coordination number of the hydroxyl oxygen atom of the adsorbed HCOOH molecule (O1) with the two –NH₂ protons (H1 and H2) of methylamine (see Figure 2). Such a CV2 choice—with respect to, e.g., an interatomic distance—offers the advantage that the exploration of the free energy surface of the reaction would not be biased by postulating the transfer of a specific proton (either H1 or H2) for the formation of a H₂O equivalent. Indeed, both H1–O1 and H2–O1 distances could have been eligible as CV2 (see Figure S7 and Paragraph 4.2, Supporting Information). As, in principle, either H1 or H2 could be transferred to O1 (see Figure S7, Supporting Information), one should have tested both O1–H1 and O1–H2 distances as CVs, making it necessary to perform either a metadynamics with three CVs, or two different metadynamics, one with the O1–H1 distance as CV2, the other with the O1–H2 distance as CV2. The definition of CV2 as the O1 coordination number did allow us to perform a single metadynamics without having to choose arbitrarily which of the two amine protons (H1 or H2) would be transferred to O1.

With this selection of CVs, we performed an ab initio metadynamics run, starting from the configuration shown in Figure 2. In such an initial state, the HCOOH molecule closest to the amine is bound to the surface via a strong Ti1–O1' interaction (2.106 Å) and a SSHB, with the O1–H3 and H3–O3 distances being 1.186 and 1.310 Å, respectively. The C1–O1 and C1–O1' distances are very similar (1.294 and 1.260 Å, respectively), in line with those found for isolated formic acid molecules adsorbed on (101) anatase.^[43,53] Also the nearby formic acid is strongly coordinated with its carbonyl oxygen to a Ti⁴⁺ center (Ti2–O2' distance: 2.130 Å), and involved in a SSHB with a surface oxygen (O2–H3' and H3'–O3' distances: 1.176 and 1.254 Å respectively).

The metadynamics simulation led to the formation of a methylformamide molecule (CH₃NHCHO) and a gas phase H₂O with a barrier of 60.0 kJ mol^{−1} (14.3 kcal mol^{−1}). A visual representation of the evolution of the system along the metadynamics run can be gathered from Movies 1a (side view) and 1b (top view).

During the metadynamics (see Movies 1a,b), the acid protons of both the adsorbed HCOOH molecules (H3 and H3') shuttle between the surface and the organic moiety, forming SSHB, thus the TiO₂ surface is acting as a protective group for the acid protons, as already reported.^[43,53] In contrast, in the final part of the simulation such a shuttling process is essentially shown only by the H3' proton.

The amine rapidly approaches with its N1 atom the formic acid C1 atom, establishing a strong interaction with the carboxyl moiety and forming an adduct characterized by a tetra-coordinated N1 atom. Interestingly, in the adduct one of the

NH₂ protons (H2) can transiently interact with the second HCOOH molecule, forming a short-lived hydrogen bond with the O2 hydroxyl oxygen. This observation suggests that the formation of the adduct has increased the Brønsted acid character of the –NH₂ protons. However, as evidenced in Movies 1a,b, the C1–N1 distance undergoes large oscillations. This behavior underlines that a proper amide bond cannot form unless the C1–O1 bond is broken. Actually, the attainment of the methylformamide product is accomplished only at the very end of the metadynamics, when an amine proton (H1) is transferred to the O1–H3 moiety, thus releasing a water molecule.

The inspection of Movies 1a,b has allowed us to gather a pictorial description of the solvent-free amidation reaction on top of the anatase (101) surface. Insight on the energetics of the process can be obtained from the free energy profile as a function of the two CVs, as shown in Figure 3. The free energy landscape presents two minima. The first one amounts to −154.6 kJ mol^{−1} (−31.9 kcal mol^{−1}). Such a relative free energy minimum is characterized by a CV1 value of ≈2.1 Å, and a CV2 value of ≈0.1, indicating that both H1 and H2 protons are still stably bonded to N1. The second and deeper minimum, −228.6 kJ mol^{−1} (−54.6 kcal mol^{−1}), corresponding to a CV1 value of ≈1.4 Å and a CV2 value of ≈0.3, is related to the reaction product—i.e., a methylformamide molecule bound to the TiO₂ surface and a “floating” water molecule. While there are not, to the best of our knowledge, experimental kinetic data to compare with, the modest free energy barrier separating these two minima, 60.0 kJ mol^{−1} (14.3 kcal mol^{−1}), is compatible with the mild experimental conditions of solvent-free TiO₂-catalyzed amidation.^[19]

Let us now discuss in detail the reaction mechanism. Such an issue could be addressed by analyzing the evolution of the CVs,

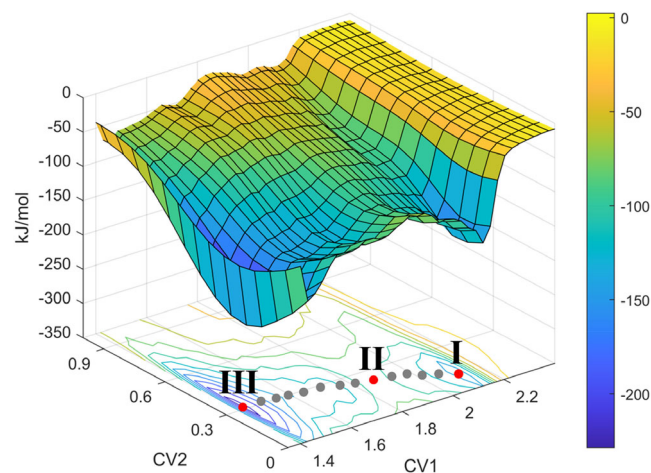


Figure 3. 3-D free energy landscape, including 2-D contour plot, for the solvent-free reaction $\text{HCOOH} + \text{CH}_3\text{NH}_2 \rightarrow \text{CH}_3\text{NHCHO} + \text{H}_2\text{O}$ on stoichiometric anatase-TiO₂(101) calculated with ab initio metadynamics on the final model system. CV1 represents the C–N distance (in Å); CV2 represents the coordination number of the HCOOH's hydroxyl oxygen with the two amine protons (see also Figure 2 CVs definition). Labels I, II, and III (and red dots) refer to the free energy landscape regions pertaining to: the first minimum, the TS, and the final state of the process, respectively. Gray dots provide a pictorial representation of the reaction path.

which is illustrated in **Figure 4**. Indeed, inspection of the instantaneous CV values along the metadynamics run reveals important features of the amide bond formation process. In the first thousand steps, the C1–N1 distance steeply decreases from its initial value (2.78 Å) to 1.37 Å, then, it rapidly grows to an average value of ≈ 3.0 Å, oscillating between 2.85 and 3.20 Å. In this region, the average coordination number (CV2) is about 0.1, indicating that both H1 and H2 are still firmly bonded to the N1 atom.

Interestingly, after 1000 steps, a change of regime can be observed. The CV1 instantaneous values—describing the N1–C1 distance—oscillate between 1.36 and 2.18 Å. The red horizontal line in **Figure 4** represents the value of a typical N–C amide bond distance (1.37 Å). Such a distance is frequently sampled in the evolution of the system between the 1000th and the 5200th step. In this region, the instantaneous values of the coordination number oscillate between 0.2 and 0.3. As evidenced by the **Movies 1a,b**, in this phase of the metadynamics, the N1 atom oscillates between a three- and a four-coordinated geometry, and a proton of the tetracoordinated N1 atom (H2) is transiently engaged in hydrogen bonding with the second HCOOH molecule (see **Figure 5**). This fact may indicate the possibility that an alternative process, involving nearby HCOOH molecules, could occur. The formation of such an intermolecular H2–O2 hydrogen bond is competing with the molecule-surface O3'–H3'–O2 SSHB. Indeed, as shown in **Figure 5a**, when H2 is strongly interacting with O2 (1.75 Å), the H3' proton is bound to a surface oxygen atom, and it is not involved in the SSHB. In contrast, when H2 is no longer hydrogen bonded to O2, the SSHB is restored (**Figure 5b**). These observations suggest that the presence of SSHBs may inhibit reaction pathways involving the transfer of $-\text{NH}_2$ protons to nearby formic acid molecules.

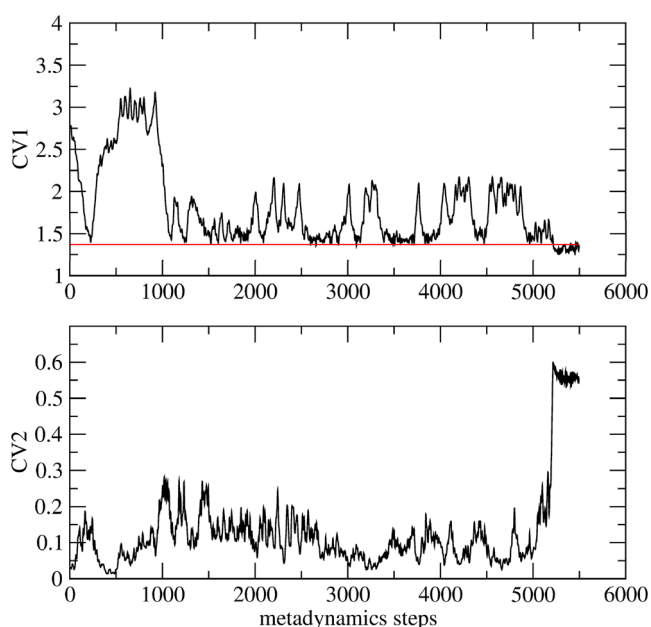


Figure 4. Evolution along the metadynamics simulation of the instantaneous collective variables CV1 (top, in Å) and CV2 (bottom). The red line in the CV1 graph (top panel) indicates a distance of 1.37 Å.

Remarkably, by inspection of the reaction top-view (**Movie 1b**), it is evident that the transient H2–O2 hydrogen bond formation is essentially due to a rotation around the Ti1–O1' bond of the HCOOH molecule involved in the adduct. Such a transient rotation is responsible of the simultaneous shortening of both C1–C2 and N1–C2 separations, which occurs between the #2500th and #3500th step (see **Figure 5c**), and causes the approaching of the H2 proton to O2. Then, the HCOOH–CH₃NH₂ adduct bounces back to its initial orientation. Moreover, the behavior of the N1–H2 and C2–O2 distances along the simulation does not show typical features of activation, such as substantial bond elongations (see **Figure 5d**).

Overall, such findings suggest that the occurrence of the amide bond formation via a competing reaction path, i.e., the transfer of a $-\text{NH}_2$ proton from the HCOOH–CH₃NH₂ moiety to the O2 atom of the nearby HCOOH, might be unlikely. In contrast, the results of the simulations with a single HCOOH (**Model 0**) may suggest a fundamental indirect role of nearby HCOOH molecules in the solvent-free amide-bond formation on TiO₂(101). Indeed, in the presence of gas-phase amine, the system with a single adsorbed HCOOH rapidly evolved into an adsorbed salt ($\text{HCOO}^- + \text{CH}_3\text{NH}_3^+$), thus suggesting that different HCOOH coverages may tune the acid strength of the adsorbed HCOOH molecules. Hence, the presence of the second adsorbed HCOOH molecule apparently decreases the acid strength of both adsorbed HCOOH, thus inhibiting salt formation and allowing for the desired condensation process.

At about the 5200th step, the instantaneous CV2 value suddenly jumps from a value of ≈ 0.1 to ≈ 0.55 , thus indicating that one H atom from the $-\text{NH}_2$ group (H1) has been transferred to the O1 atom, leading to the formation of a H₂O molecule and an amide moiety, as detectable by the simultaneous shortening of the N1–C1 distance (CV1), see also **Movies 1a,b**. A concerted (one-step) amide bond formation mechanism clearly emerges from these data. Further analyses corroborating this picture are reported in paragraph S4.3, Supporting Information. In particular, the evolution of the O1–H1 and O1–H3 distances (**Figure S8**) clearly evidences the formation of a new H1–O1–H3 molecule, which occurs concomitantly to the CV2 jump (**Figure 4**). Moreover, the H1–O1–H3 angle and the H2–N1–C1–O1' dihedral angle (**Figure S9**) reach the values pertaining to the reaction products only in the final part of the simulation, concurrently with the formation of the O1–H1 and C1–N1 bonds.

Once the amide is formed (5200th step), the metadynamics algorithm starts to explore the repulsive part of the C1–N1 interaction, as suggested by the further shortening of the N1–C1 distance (≈ 1.33 Å, see **Figure 4**) as well as by the steep free energy increase at short CV1 distances (see **Figure 4**).

The TS can be located by considering the region corresponding to the sharp rise of the CV2 variable—more specifically, a 25-step interval comprised between step #5193 (CV2 = 0.26) and step #5217 (CV2 = 0.60). Although we arbitrarily chose as TS the configuration corresponding to the 0.4 value of the instantaneous CV2 (step #5204), it should be stressed that all metadynamics steps in this interval provide a very similar picture of the geometrical and electronic features of the activated complex.

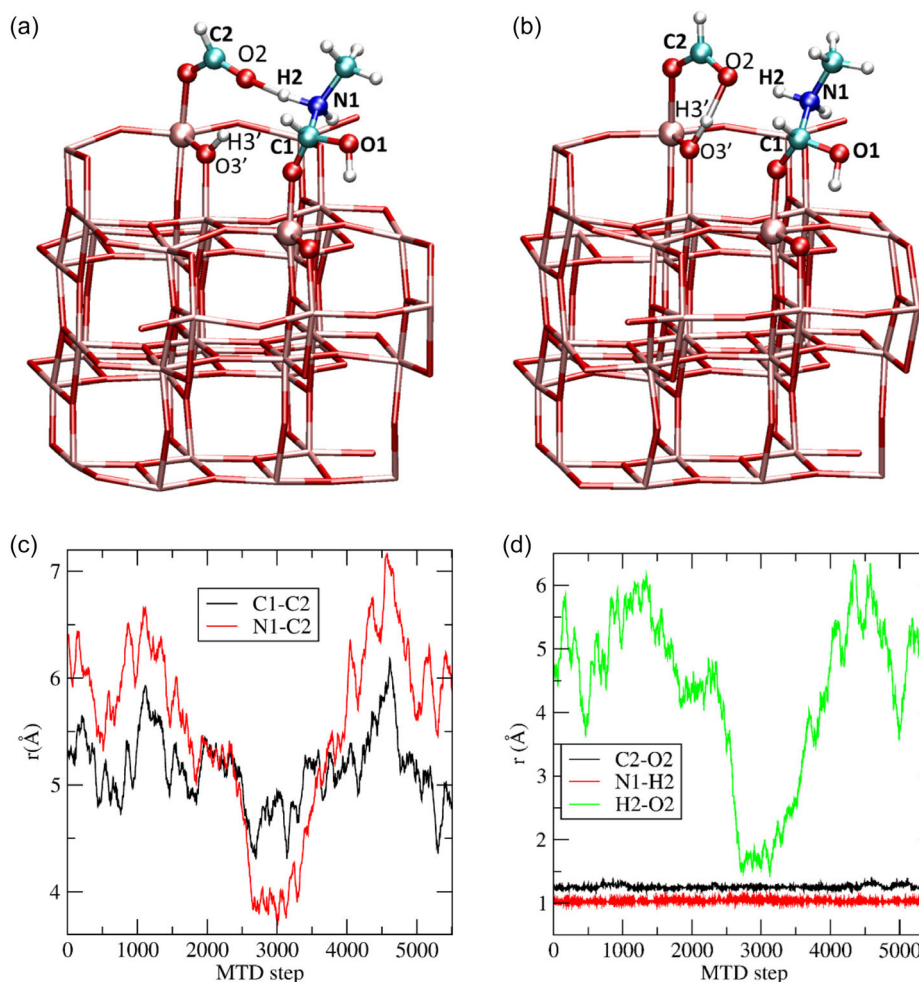


Figure 5. a,b): Graphical representation of two configurations pertaining to the reaction path, which highlight: a) the transient hydrogen bond between the hydroxyl oxygen O2 and the H2 atom of the $\text{CH}_3\text{NH}_2\text{-HCOOH}$ adduct, b) the SSHB between the hydroxyl oxygen O2 and the H3' proton, linked to a surface oxygen. Color codes as in Figure 2. c,d): Evolution along the metadynamics (MTD) simulation of: c) C1–C2 and N1–C2 distances; d) C2–O2, N1–H2, and H2–O2 distances.

The TS geometry (see **Figure 6**) is characterized by a 4-center ring structure involving the N1, H1, O1, and C1 atoms. The O1–H3 hydroxyl group points outside the ring structure but it is not involved in SSHB with the surface. Interestingly, the H1 atom is shared between the amine nitrogen and the hydroxyl oxygen, with the H1–N1 and H1–O1 distances amounting to 1.261 and 1.224 Å, respectively (Figure 6a). The C1–N1 separation is 1.476 Å—hence, still longer than a typical amide bond. Nevertheless, the C1–O1 distance (1.487 Å) elongates significantly with respect to the starting configuration, suggesting the weakening of such a bond. Moreover, the C1–O1 distance becomes much longer than the C1–O1' one (1.288 Å). It should be noticed that a similar geometrically strained 4-center ring has been obtained in the TS calculated for the first step of the peptide bond formation between two glycine molecules on regular (101) anatase surface.^[16] In contrast, a two-step mechanism (nucleophilic attack followed by dehydration) was predicted for the condensation of the two aminoacids.^[16] In the present case, the formation of the reaction products occurs in a single concerted step.

Further insight on the TS is provided by electronic structure analysis. Indeed, a Wannier orbital localized on the 4-center moiety exhibits bonding character with respect to H1–O1, and anti-bonding character with respect to H1–N1 (Figure 6b), indicating the incipient formation of the H1–O1 bond accompanied by the breaking of the H1–N1 bond.

Remarkably, the activated complex is strongly coordinated to the TiO_2 surface (Ti1–O1' distance: 1.997 Å), thus supporting the idea of a stabilizing role of the titania surface in the formation of the activated complex. Indeed, a closer analysis of the electronic structure evidenced Wannier orbitals involving both the Ti1 site and the adsorbed $\text{HCOOH-CH}_3\text{NH}_2$ complex, which suggest an appreciable covalent character for the Ti1–O1' interaction (**Figure 7**). Such Wannier orbitals are mainly localized on the O1'–C1 atoms, but they also extend over the Ti1 center, suggesting donation of electronic density from the adsorbed complex toward the empty d-states of the surface cation. These results, in line with previous findings on aminoacid condensation,^[16] support the intuitive argument that the Lewis

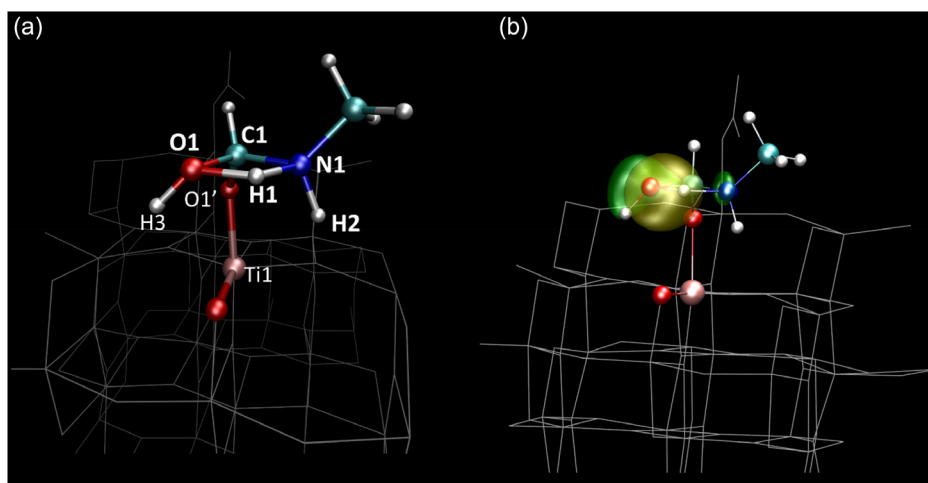


Figure 6. Graphical representation of the TS structure, highlighting: a) the four-center N1–H1–O1–C1 ring assisting the transfer of the H1 proton from the amine N1 atom to the carboxylate O1 atom; b) the Wannier orbital associated to the formation of the water molecule via proton transfer from the -NH_2 group to the O1–H3 moiety. The reaction center is in ball-and-stick representation (atom color codes as in Figure 2), while the rest of the simulation system is shown as gray sticks. The yellow and green shaded regions represent positive and negative phases of the Wannier orbital localized on the forming H_2O molecule.

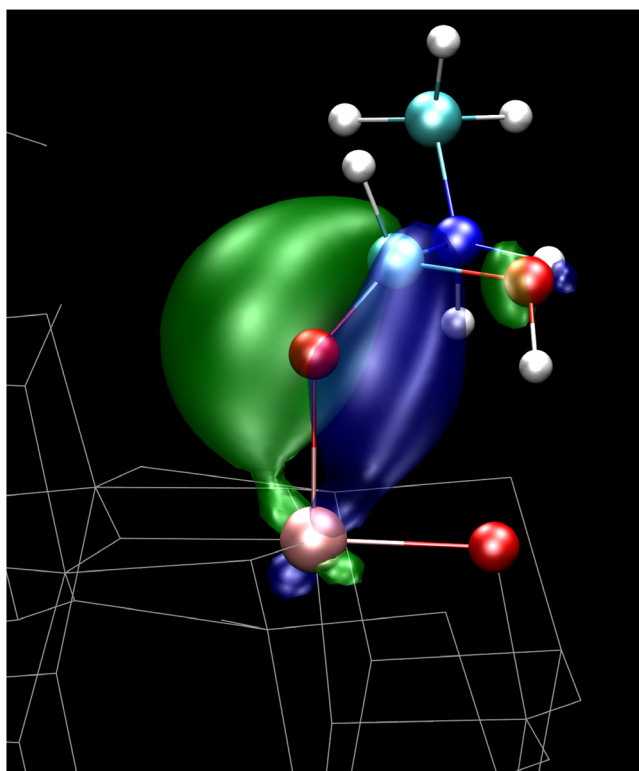


Figure 7. Graphical representation of the TS structure, highlighting one of the Wannier orbitals associated to the interaction of the $\text{HCOOH-CH}_3\text{NH}_2$ complex with the anatase (101) surface. The reaction center is in ball-and-stick representation (atom color codes as in Figure 2), while the rest of the simulation system is shown as gray sticks. The blue and green shaded regions represent positive and negative phases of the Wannier orbital.

acid character of the anatase Ti^{4+} sites can increase the electrophilicity of an adsorbed carboxy species,^[19] thus making its carbon atom prone to a direct nucleophilic attack.

Also notably, the state shown in Figure 7 has π -bonding character with respect to the three-center Ti1-O1'-C1 bond, and σ -antibonding character with respect to the C1-O1 bond, which should be cleaved in the amidation process. These findings corroborate the hypothesis that standard Ti^{4+} sites on regular stoichiometric anatase (101) surfaces can catalyze the cleavage of the carboxyl C–O bond, i.e., the rate-determining step for dehydration and amide bond formation—by stabilizing a TS featuring a cyclic N–H–O–C moiety (Figure 6 and 7). Such a ring structure—although geometrically strained—appears to be functional in promoting the transfer of a -NH_2 proton to the hydroxyl oxygen of the carboxylic acid.

The deepest free energy minimum, associated to the final state of the process—i.e., the reaction products—is illustrated in Figure 8. A stable gas phase water molecule is formed, characterized by O1–H3 and O1–H1 distances of 0.956 and 0.946 Å, respectively, while its bond angle is 105.2°. The C1–N1 separation (1.352 Å) indicates the formation of an actual amide bond, characterized by a double bond character. Moreover, the C1–O1' distance (1.196 Å)—is typical of a C–O carbonyl bond, and the molecule is nearly planar (H2-N1-C1-O1' dihedral angle = 0.5°), thus underlining the attainment of the methylformamide product (Figure 8a). This picture is further supported by the electronic structure analysis, evidencing a π -bonding component on the C1–N1 moiety (Figure 8b). Although methylformamide remains coordinated to Ti1 (Ti1-O1' distance = 2.284 Å) after the release of the water molecule, such a distance is longer with respect to the Ti1–O1' separation in both the starting metadynamics configuration (2.106 Å) and in the TS (1.997 Å). This comparison indicates that the amide– TiO_2 interaction

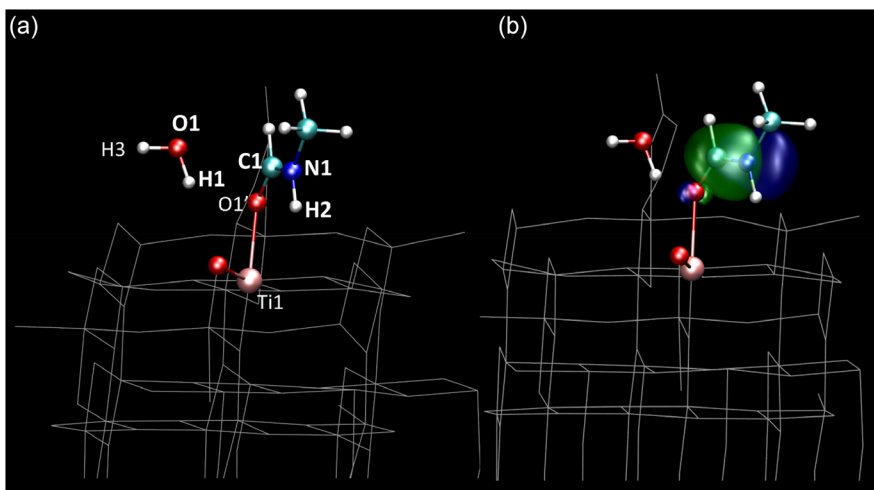


Figure 8. Graphical representation of the structure of the reaction products, highlighting: a) the newly formed H₂O molecule and the methylformamide, coordinated to the Ti1 surface site; b) the Wannier molecular orbital associated to the π -component of the C1–N1 amide bond. The reaction products are in ball-and-stick (atom color codes as in Figure 2), while the rest of the simulation system is shown as gray sticks. The blue and green shaded regions represent positive and negative phases of the Wannier orbital localized on the C1–N1 bond.

should be weaker than the HCOOH–TiO₂ interaction at the start of the amidation process, hence suggesting that the release of the amide product from the TiO₂ surface might be easier than the desorption of the HCOOH reactant. Moreover, such a trend of the Ti1–O1' distance—and specifically, the particularly short Ti1–O1' bond in the TS, further underlines the critical impact of the surface Ti⁴⁺ sites in stabilizing a TS geometry involving a tensioned 4-center ring (see Figure 6 and 7).

Finally, to investigate the equilibrium behavior of the reaction products at the temperature conditions of the amidation experiments, we carried out an AIMD simulation starting from the final configuration of the metadynamics run for 10 ps elapsed time (see Movie S5 and paragraph S4.4, Supporting Information). As evidenced by Movie S5, the methylformamide molecule remains coordinated to the Ti1 site via a strong Ti–O interaction, being the average Ti1–O1_{amide} distance 2.09 Å, with standard deviation of 0.07 Å (Figure S10, Supporting Information).

Notably, the water molecule gradually moves away from methylformamide, and, at the end of the simulation, it is fully desorbed from the surface. This behavior is in line with the experimental IR data on the solvent-free amide-bond formation on TiO₂, indicating the absence of water on the TiO₂ surface after the amidation reaction.^[19] Importantly, the postamidation water desorption, shown herein, suggests that the produced H₂O has a low probability of influencing the reactivity of other HCOOH–CH₃NH₂ pairs that could be co-present on top of the TiO₂ surface.

So far we have reported on the solvent-free direct condensation process $\text{HCOOH} + \text{CH}_3\text{NH}_2 \rightarrow \text{CH}_3\text{NHCHO} + \text{H}_2\text{O}$ on stoichiometric (101) anatase facets. While this surface is the most abundant in TiO₂ nanoparticles, other phases (rutile) or types of minority facets could, in principle, catalyze such a reaction. Rutile is a minority component of the P25 nanopowders adopted in the solvent-free amidation.^[19] P25 is constituted by 20% rutile and 80% anatase, but the specific surface area of rutile is only the 7%.^[48]

Recent studies^[37,54] on a related process (HCOOH dehydration catalyzed by TiO₂, which also involves the formation of a water molecule) suggest a complex scenario for the catalytic effect of TiO₂(110) rutile with respect to regular TiO₂(101) anatase facets. While at high temperatures (533–563 K), the two systems have comparable activity, at lower temperatures (423–463 K), the catalytic effect of TiO₂(110) rutile is much lower than that shown by anatase(101). Moreover, in the same studies, the activity of both catalysts was reported to be independent of the presence of surface defects like, e.g., oxygen vacancies and/or isolated titanols. In principle, these results do not exclude a catalytic effects of rutile on the amidation process, however, they strongly support the idea that at temperatures as low as 320 K, the contribution of rutile should be relatively modest. Also, these results^[37,54] suggest that HCOOH reactivity on TiO₂ is not strictly dependent on defects.

Particularly relevant in this context is the finding that, by comparing the catalytic activities of TiO₂-P25 and 100% anatase-TiO₂ nanoparticles in the solvent-free condensation of nonactivated amino acids, it has been found that the reaction does not require peculiar defects such, e.g., oxygen vacancies, or sites on minority facets and/or highly energetic surface terminations, but it takes place on the most abundant anatase-TiO₂(101) facets.^[22]

Whereas the exploration of the activity of minority sites/facets/phases in TiO₂ nanoparticles may increase our knowledge basis on their role in catalysis, in the present case, it may be reasonably argued that the simulation of solvent-free amide bond formation catalyzed by stoichiometric anatase(101) surfaces should represent the very large majority of such reactive events on TiO₂ nanoparticles.

3. Conclusion

The aim of this study was to gather atomistic-level insight on solvent-free direct amide bond formation between carboxylic

acids and amines on anatase TiO₂(101) surfaces. This reaction was reported to occur at mild temperature conditions on TiO₂-P25 nanoparticles, however, its mechanistic and energetic details were unknown. By modeling the process via DFT-based AIMD and metadynamics, the free energy surface of the reaction was investigated. The predicted reaction mechanism is of the Eley–Rideal type, and involves a direct nucleophilic attack of gas-phase methylamine on the carbonyl C atom of a formic acid molecule already adsorbed on the titania surface. Formation of the amide bond and liberation of a water molecule occur concertedly in a single step. The TS of the reaction has been identified as the formation of an activated complex between methylamine and adsorbed formic acid, characterized by a strained four-center N–H–O–C ring moiety. Such a four-center ring assists the transfer of an amine proton to the HCOOH hydroxyl oxygen, producing methylformamide coordinated to a surface Ti⁴⁺ site and liberating gas-phase water. The TiO₂(101) anatase surface plays a key role in stabilizing the TS via a strong Ti–O–C interaction with partially covalent character.

Our findings indicate that the solvent-free amidation process can occur with a modest activation barrier (14.3 kcal mol⁻¹) on canonical Ti⁴⁺ and O²⁻ sites on stoichiometric anatase(101) surfaces. Even though, to the best of our knowledge, no experimental kinetic data on this reaction has been reported so far to compare with, the calculated barrier aligns with the mild experimental conditions used in direct amide bond syntheses on TiO₂ nanoparticles.

Additionally, by exploring the effect of different degrees of HCOOH coverages, this work reveals the indirect but relevant role of nearby coadsorbed HCOOH molecules on the amide-bond formation reaction. Namely, the copresence of HCOOH molecules on the TiO₂ surface might help to decrease their acid strength with respect to an isolatedly adsorbed formic acid. Whereas the system with a single adsorbed HCOOH rapidly evolves into an adsorbed salt in the presence of amine (HCOO⁻ + CH₃NH₃⁺), such parasite salt-formation process—which burden direct amide-bond formation routes in the absence of protective groups—does not take place when a second HCOOH molecule is coadsorbed.

Concerning the fate of the side product, molecular H₂O, we have shown that the water molecule rapidly desorbs from the surface, in line with the available experimental data. The rapid post-amidation water desorption supports the idea that the produced H₂O should not affect significantly the behavior of other HCOOH–CH₃NH₂ pairs on top of the TiO₂ surface.

In conclusion, this study discloses relevant microscopic aspects of the catalytic action of nondefective Ti centers on (101) anatase in amide-bond formation processes. This reaction can occur without the need of specific surface defects, whose nature and concentration might depend on particular procedures adopted in the catalyst synthesis. Hence, the active role of the (101) anatase surface in this process can be ascribed to the vast majority of the exposed Ti sites on anatase nanoparticles. Remarkably, the presence of a high density of catalytically active sites could be beneficial for scaling purposes.

In perspective, further insight may be gathered by investigating whether defects, like titanols, oxygen vacancies, high energy sites on nanoparticles' edges and corners, or even different TiO₂ phases like rutile, might be able to catalyze direct-solvent-free

amidation reactions, and to assess how their reactivity compares with that shown by the regular anatase TiO₂(101) facets.

From a broader viewpoint, the results presented in this work may contribute to provide momentum to the exploration of economically and environmentally benign metal oxide (nano)materials as potential catalysts for solvent-free direct amide syntheses.

4. Experimental Section

General Computational Details: The solvent-free direct amidation process, object of the present study, was investigated on two model systems, differing for the degree of HCOOH coverage of the anatase TiO₂(101) surface.

In the actual solvent-free direct amidation experiment, pentylamine was dosed from the gas phase on a TiO₂ surface already partially covered by HCOOH.^[19] In our models, for the sake of computational economy, we used methylamine (CH₃NH₂). A preliminary model (HCOOH@TiO₂ + CH₃NH₂, denoted Model 0) was constituted by an anatase TiO₂(101) slab, one adsorbed HCOOH molecule, and one gas phase CH₃NH₂ molecule per simulation unit cell. In the final model ((HCOOH)₂@TiO₂ + CH₃NH₂), the degree of HCOOH coverage was doubled with respect to Model 0.

In both models, the bare (101) surface of anatase TiO₂ was modeled similarly as in ref. [43]. The periodically repeated slab employed herein (Ti₃₆O₇₂), formed by six Ti₆O₁₂ layers (surface area: 10.349 × 11.355 Å² in the *xy* plane), provides a good description of the adsorption of probe molecules on TiO₂(101) at both low- and high-coverage conditions, as shown in previous investigations.^[43,48,55,56] In all the calculations of the present work, a vacuum space of 14 Å along the *z* direction was used with the purpose to minimize interactions between images. The atoms of the bottom Ti₆O₁₂ layer were held fixed. In all the performed calculations, the PBE^[57] approximation to DFT, combined with empirical dispersion corrections,^[58] was employed.^[59] This scheme for the electronic structure description yielded a good representation of the interaction of molecules with oxide materials at finite temperature conditions in AIMD simulations.^[60–64] Norm-conserving pseudopotentials were adopted for the electron-cores interactions, along with the nonlinear core correction protocol for Ti (considered as Ti⁴⁺).^[65–67] Plane-wave (PW) basis sets were adopted throughout, by selecting as cutoffs for the PW expansion of wavefunctions and electronic density 80 and 320 Ry, respectively, on the basis of convergence tests performed in previous investigations on different anatase TiO₂(101) models.^[43] The size of the simulation cell enabled a Γ -point-based calculation. Convergence toward Brillouin Zone sampling was already validated in previous investigations against the Ti–O bond length.^[48] Tests of *k*-points sampling vs. binding energy were here performed for a water molecule adsorbed on the TiO₂(101) slab (see Section S2, Supporting Information). The results indicate that the difference between adsorption energies computed using only the Γ -point and a 3 × 3 × 1 *k*-point mesh amounts to about 1%. Hence, the energy convergence can be considered satisfactory even by including only the Γ -point in the Brillouin Zone sampling.

All the AIMD simulations were carried out in the NVT ensemble, with Nose–Hoover chain thermostats,^[68,69] by integrating the Car–Parrinello equations of motion^[44,45] with a time step of 5 atomic units (a.u.) (0.121 fs) and a fictitious mass of the wavefunction's coefficients of 500 a.u. The target temperature was set to 320 K.

The free energy surface for the formation of the amide from HCOOH adsorbed on (101) anatase and gas phase methylamine was investigated by combining the AIMD approach^[44,45] with the metadynamics method.^[46,47] Preliminary studies were also performed, by employing standard AIMD, AIMD-metadynamics, and the AIMD-BM approach.^[49] Both metadynamics and BM are enhanced sampling approaches commonly used to simulate reactive processes, which can be considered “rare events” on the timescale of AIMD simulations. More specifically, metadynamics is based on the definition of a history dependent potential, that is added to the actual potential of the system, thus allowing the system to

overcome free energy barriers and to explore the free energy surface as a function of specific reaction coordinates denoted as “collective variables” (CVs).^[46] In the BM approach, instead of CVs, a reaction coordinate related to geometric parameters is sampled by performing a series of AIMD simulations (the path, see e.g. ref. [70]). In each simulation of the path, the reaction coordinate (or “constraint”) is fixed at a selected value, and the simulation is run until convergence of the constraint force.^[49,50] The free energy profile is then computed by integration of the constraint forces obtained along the path.^[49,50,71]

One HCOOH Adsorbed on Anatase TiO₂(101) Slab Plus a Gas Phase CH₃NH₂: Model 0, constituted by one HCOOH molecule adsorbed on the TiO₂(101) slab (HCOOH@TiO₂(101)), and a gas phase CH₃NH₂ molecule, was built by starting from the minimum energy structure of the HCOOH@TiO₂(101) system reported in ref. [43], and placing a CH₃NH₂ molecule above the surface, at a distance of ≈ 4 Å from the carbon atom of the adsorbed formic acid molecule. Subsequently, the system was subjected to 5 ps equilibration with AIMD^[44] at a target temperature of 320 K before performing a combined AIMD-BM^[49] simulation. Also, a metadynamics simulation on this system was performed. Finally, a standard AIMD run at 320 K (elapsed time = 5 ps) was performed as well. Further details on Model 0 are reported in paragraph S1.1 and Section S3, Supporting Information.

Two HCOOH Adsorbed on Anatase TiO₂(101) Slab Plus a Gas Phase CH₃NH₂: The building of the final model ((HCOOH)₂@TiO₂ + CH₃NH₂) required, as a preliminary step, the determination of the most energetically convenient geometry for the adsorption of two HCOOH molecules on the TiO₂(101) slab. A search of the minimum energy structure of the TiO₂(101) model slab bearing two adsorbed HCOOH molecules ((HCOOH)₂@TiO₂) was performed by considering six models (see paragraphs S1.2 and S4.1, Supporting Information). The resulting minimum energy structure was used to build the final model for the simulation of the amidation process ((HCOOH)₂@TiO₂ + CH₃NH₂).

The final model system was composed by the aforementioned TiO₂(101) slab, two adsorbed formic acid molecules (separated by 5.46 Å), and one methylamine molecule in the gas phase. The choice of modeling two adsorbed HCOOH molecules on the TiO₂(101) slab was suggested by the results obtained on the system featuring only one HCOOH molecule adsorbed on the TiO₂(101) slab (see section S3, Supporting Information), as well as by the reported coverage conditions at which the direct amidation experiments were conducted.^[19]

Such a molecule was initially positioned with its N atom at 5 Å from the top layer of the minimum energy structure of the (HCOOH)₂@TiO₂ system (see paragraph S4.1, Supporting Information). Also, the amine N atom was equally separated by the same distance (5 Å) from the two C atoms of the two adsorbed HCOOH. Such a system was equilibrated via AIMD (elapsed simulation time: 5 ps) at 320 K, in line with the conditions at which the direct amide synthesis experiments were performed on TiO₂ ($T = 323$ K).^[19] The final structure obtained from the equilibration run was employed as starting configuration for the metadynamics run.

In the present case, as CVs for the metadynamics simulation, we selected the distance between the N1 atom of the amine and the C1 atom of an adsorbed formic acid molecule (CV1), and the coordination number of the O1 atom of the same HCOOH molecule with the two -NH₂ protons (CV2) (see Figure 2). Further details about the choice and the definition of the selected collective variables are reported in paragraph S1.4, Supporting Information.

The CVs dynamics were performed in the frame of the extended Lagrangean formalism using the Lagrange–Langevin algorithm^[51,52,72] with friction of 0.001 a.u. and target temperature of 320 K. The values of the Gaussian hills’ parameters (i.e., perpendicular width and height) adopted in the metadynamics run were 0.1 and 0.001 a.u., respectively. A total of 5508 metadynamics steps were performed. The free energy profile obtained from metadynamics was reconstructed using the VRECO code^[73] and then smoothed by using a Savitzky–Golay filter,^[74] as implemented in MATLAB, to obtain the plots shown in Figure 3.

Insight on the electronic properties of the systems was gathered via inspection of the maximally localized Wannier orbitals.^[75–77] These functions are obtained via a unitary transformation of Bloch orbitals, and

represent a broadly adopted method to investigate the electronic structure of periodic systems, as they provide a real-space localized description of one-particle orbitals, and thus an intuitive picture for chemical bonding.^[73–75]

All calculations presented in this study were run with the CPMD code.^[78,79]

Supporting Information

Supporting Information is available from the Wiley Online Library or from the author.

Acknowledgements

The authors acknowledge Insubria University for financial support (FAR 2023) and Dr. Mario Oriani for technical assistance.

Conflict of Interest

The authors declare no conflict of interest.

Author Contributions

Ettore Fois: Conceptualization (equal); Data curation (equal); Formal analysis (equal); Funding acquisition (equal); Investigation (equal); Methodology (equal); Project administration (equal); Resources (equal); Software (equal); Supervision (equal); Validation (equal); Visualization (equal); Writing—original draft (equal); Writing—review & editing (equal).
Gloria Tabacchi: Conceptualization (equal); Data curation (equal); Formal analysis (equal); Funding acquisition (equal); Investigation (equal); Methodology (equal); Project administration (equal); Resources (equal); Software (equal); Supervision (equal); Validation (equal); Visualization (equal); Writing—original draft (equal); Writing—review & editing (equal).

Data Availability Statement

The data that support the findings of this study are openly available in [figshare] at [https://doi.org/10.6084/m9.figshare.26132809.v1], reference number [26132809].

Keywords

amidation, density functional theory calculations, heterogeneous catalysis, metadynamics, titanium dioxide

Received: July 1, 2024
Revised: October 8, 2024
Published online:

- [1] V. R. Pattabiraman, J. W. Bode, *Nature* **2011**, *480*, 471.
- [2] C. L. Allen, J. M. J. Williams, *Chem. Soc. Rev.* **2011**, *40*, 3405.
- [3] H. Ishitani, K. Takeno, M. Sasaya, S. Kobayashi, *Catal. Sci. Technol.* **2023**, *13*, 5536.
- [4] D. J. C. Constable, P. J. Dunn, J. D. Hayler, G. R. Humphrey, J. L. Leazer, R. J. Linderman, K. Lorenz, J. Manley, B. A. Pearlman, A. Wells, A. Zaks, T. Y. Zhang, *Green Chem.* **2007**, *9*, 411.
- [5] N. Martín, F. G. Cirujano, *Catal. Commun.* **2022**, *164*, 106420.
- [6] H. Lundberg, F. Tinnis, N. Selander, H. Adolfsson, *Chem. Soc. Rev.* **2014**, *43*, 2714.

- [7] M. C. Bryan, P. J. Dunn, D. Entwistle, F. Gallou, S. G. Koenig, J. D. Hayler, M. R. Hickey, S. Hughes, M. E. Kopach, G. Moine, P. Richardson, F. Roschangar, A. Steven, F. J. Weiberth, *Green Chem.* **2018**, *20*, 5082.
- [8] M. Kumar, S. Sharma, K. Thakur, O. S. Nayal, V. Bhatt, M. S. Thakur, N. Kumar, B. Singh, U. Sharma, *Asian J. Org. Chem.* **2017**, *6*, 342.
- [9] M. Amirsoleimani, M. A. Khalilzadeh, D. Zareyee, *Reac Kinet Mech Cat* **2020**, *131*, 859.
- [10] K. Komura, Y. Nakano, M. Koketsu, *Green Chem.* **2011**, *13*, 828.
- [11] I. A. Lázaro, R. S. Forgan, F. G. Cirujano, *Dalton Trans.* **2022**, *51*, 8368.
- [12] F. de Azambuja, A. Loosen, D. Conic, M. van den Besselaar, J. N. Harvey, T. N. Parac-Vogt, *ACS Catal.* **2021**, *11*, 7647.
- [13] K. P. Patel, E. M. Gayakwad, G. S. Shankarling, *ChemistrySelect* **2020**, *5*, 8295.
- [14] M. B. M. Reddy, S. Ashoka, G. T. Chandrappa, M. A. Pasha, *Catal Lett* **2010**, *138*, 82.
- [15] M. Hosseini-Sarvari, E. Sodagar, M. M. Doroodmand, *J. Org. Chem.* **2011**, *76*, 2853.
- [16] S. Pantaleone, P. Ugliengo, M. Sodupe, A. Rimola, *Chem. Eur. J.* **2018**, *24*, 16292.
- [17] A. Rimola, M. Fabbiani, M. Sodupe, P. Ugliengo, G. Martra, *ACS Catal.* **2018**, *8*, 4558.
- [18] S. Nagarajan, P. Ran, P. Shanmugavelan, M. Sathishkumar, A. Ponnuswamy, K. S. Nahm, G. G. Kumar, *New J. Chem.* **2012**, *36*, 1312.
- [19] C. Deiana, Y. Sakhno, M. Fabbiani, M. Pazzi, M. Vincenti, G. Martra, *ChemCatChem* **2013**, *5*, 2832.
- [20] N. G. Petrik, Y. Wang, B. Wen, Y. Wu, R. Ma, A. Dahal, F. Gao, R. Rousseau, Y. Wang, G. A. Kimmel, A. Selloni, Z. Dohnálek, *J. Phys. Chem. C* **2021**, *125*, 7686.
- [21] S. Selçuk, A. Selloni, *J. Phys. D: Appl. Phys.* **2017**, *50*, 273002.
- [22] M. Fabbiani, M. Pazzi, M. Vincenti, G. Tabacchi, E. Fois, G. Martra, *J. Nanosci. Nanotechnol.* **2018**, *18*, 5854.
- [23] G. Martra, C. Deiana, Y. Sakhno, I. Barberis, M. Fabbiani, M. Pazzi, M. Vincenti, *Angew. Chem. Int. Ed.* **2014**, *53*, 4671.
- [24] A. Vittadini, A. Selloni, F. P. Rotzinger, M. Grätzel, *J. Phys. Chem. B* **2000**, *104*, 1300.
- [25] X. Gong, A. Selloni, A. Vittadini, *J. Phys. Chem. B* **2006**, *110*, 2804.
- [26] M. Xu, H. Noei, M. Buchholz, M. Muhler, C. Wöll, Y. Wang, *Catal. Today* **2012**, *182*, 12.
- [27] D. C. Grinter, M. Nicotra, G. Thornton, *J. Phys. Chem. B* **2012**, *116*, 11643.
- [28] F. Nunzi, F. De Angelis, *J. Phys. Chem. C* **2011**, *115*, 2179.
- [29] K. L. Miller, J. L. Falconer, J. W. Medlin, *J. Catal.* **2011**, *278*, 321.
- [30] A. Mattsson, L. Österlund, *J. Phys. Chem. C* **2010**, *114*, 14121.
- [31] A. Mattsson, S. Hu, K. Hermansson, L. Österlund, *J. Chem. Phys.* **2014**, *140*, 034705.
- [32] M. J. Tillotson, P. M. Brett, R. A. Bennett, R. Grau-Crespo, *Surf. Sci.* **2015**, *632*, 142.
- [33] D. Meroni, L. Lo Presti, G. Di Liberto, M. Ceotto, R. G. Acres, K. C. Prince, R. Bellani, G. Soliveri, S. Ardizzone, *J. Phys. Chem. C* **2017**, *121*, 430.
- [34] L. Kou, T. Frauenheim, A. L. Rosa, E. N. Lima, *J. Phys. Chem. C* **2017**, *121*, 17417.
- [35] Y. Li, Y. Gao, *Langmuir* **2018**, *34*, 546.
- [36] Y. Wang, B. Wen, A. Dahal, G. A. Kimmel, R. Rousseau, A. Selloni, N. G. Petrik, Z. Dohnálek, *J. Phys. Chem. C* **2020**, *124*, 20228.
- [37] S. Kwon, T. C. Lin, E. Iglesia, *J. Phys. Chem. C* **2020**, *124*, 20161.
- [38] K. Sellschopp, G. B. Vonnun-Feldbauer, *Nanoscale* **2023**, *15*, 16967.
- [39] F. Brandalise Nunes, N. Comini, J. T. Diulus, T. Huthwelker, M. Iannuzzi, J. Osterwalder, Z. Novotny, *J. Phys. Chem. Lett.* **2023**, *14*, 3132.
- [40] M. R. Mulay, N. Martsinovich, *Mole. Phys.* **2023**, *121*, e2165981.
- [41] E. Fallacara, *Ph.D. Thesis*, Sorbonne Université **2022**.
- [42] D. Forrer, A. Vittadini, *Molecules* **2022**, *27*, 6538.
- [43] G. Tabacchi, M. Fabbiani, L. Mino, G. Martra, E. Fois, *Angew. Chem. Int. Ed.* **2019**, *58*, 12431.
- [44] R. Car, M. Parrinello, *Phys. Rev. Lett.* **1985**, *55*, 2471.
- [45] D. Marx, J. Hutter, *Ab Initio Molecular Dynamics*, Cambridge University Press, Cambridge **2009**.
- [46] A. Laio, M. Parrinello, *Proc. Natl. Acad. Sci. U.S.A.* **2002**, *99*, 12562.
- [47] M. Iannuzzi, A. Laio, M. Parrinello, *Phys. Rev. Lett.* **2003**, *90*, 4.
- [48] C. Deiana, M. Minella, G. Tabacchi, V. Maurino, E. Fois, G. Martra, *Phys. Chem. Chem. Phys.* **2013**, *15*, 307.
- [49] E. A. Carter, G. Ciccotti, J. T. Hynes, R. Kapral, *Chem. Phys. Lett.* **1989**, *156*, 472.
- [50] G. Ciccotti, R. Kapral, A. Sergi, *Handbook of Materials Modeling*, Springer Netherlands, Dordrecht **2005**, pp. 1597–1611.
- [51] A. Laio, F. L. Gervasio, *Rep. Prog. Phys.* **2008**, *71*, 126601.
- [52] A. Barducci, M. Bonomi, M. Parrinello, *WIREs Comput. Mole. Sci.* **2011**, *1*, 826.
- [53] E. Fallacara, F. Finocchi, M. Cazzaniga, S. Chenot, S. Stankic, M. Ceotto, *Angew. Chem. Int. Ed.* **2024**, e202409523.
- [54] S. Kwon, T. C. Lin, E. Iglesia, *J. Catal.* **2020**, *383*, 60.
- [55] C. Deiana, G. Tabacchi, V. Maurino, S. Coluccia, G. Martra, E. Fois, *Phys. Chem. Chem. Phys.* **2013**, *15*, 13391.
- [56] C. Deiana, E. Fois, G. Martra, S. Narbey, F. Pellegrino, G. Tabacchi, *ChemPhysChem* **2016**, *17*, 1956.
- [57] J. P. Perdew, K. Burke, M. Ernzerhof, *Phys. Rev. Lett.* **1996**, *77*, 3865.
- [58] S. Grimme, *J. Comput. Chem.* **2006**, *27*, 1787.
- [59] L. Bigiani, D. Zappa, D. Barreca, A. Gasparotto, C. Sada, G. Tabacchi, E. Fois, E. Comini, C. Maccato, *ACS Appl. Mater. Interfaces* **2019**, *11*, 23692.
- [60] E. Fois, A. Gamba, C. Medici, G. Tabacchi, S. Quartieri, E. Mazzucato, R. Arletti, G. Vezzalini, V. Dmitriev, *Microporous Mesoporous Mater.* **2008**, *115*, 267.
- [61] R. Arletti, E. Fois, L. Gigli, G. Vezzalini, S. Quartieri, G. Tabacchi, *Angew. Chem., - Int. Ed.* **2017**, *56*, 2105.
- [62] G. Tabacchi, G. Calzaferri, E. Fois, *Chem. Commun.* **2016**, *52*, 11195.
- [63] L. Bigiani, T. Andreu, C. Maccato, E. Fois, A. Gasparotto, C. Sada, G. Tabacchi, D. Krishnan, J. Verbeeck, J. R. Morante, D. Barreca, *J. Mater. Chem. A* **2020**, *8*, 16902.
- [64] G. Tabacchi, I. Armenia, G. Bernardini, N. Masciocchi, A. Guagliardi, E. Fois, *ACS Appl. Nano Mater.* **2023**, *6*, 12914.
- [65] N. Troullier, J. L. Martins, *Phys. Rev. B* **1991**, *43*, 1993.
- [66] D. Hamann, M. Schlüter, C. Chiang, *Phys. Rev. Lett.* **1979**, *43*, 1494.
- [67] L. Kleinman, D. M. Bylander, *Phys. Rev. Lett.* **1982**, *48*, 1425.
- [68] S. Nosé, *J. Chem. Phys.* **1984**, *81*, 511.
- [69] W. G. Hoover, *Phys. Rev. A* **1985**, *31*, 1695.
- [70] D. Barreca, E. Fois, A. Gasparotto, C. Maccato, M. Oriani, G. Tabacchi, *Molecules* **2021**, *26*, 1988.
- [71] J.-P. Ryckaert, G. Ciccotti, H. J. C. Berendsen, *J. Comput. Phys.* **1977**, *23*, 327.
- [72] C. Micheletti, A. Laio, M. Parrinello, *Phys. Rev. Lett.* **2004**, *92*, 170601.
- [73] N. N. Nair, GitHub - Vreco_CPMD: CPMD Free Energy Surface Reconstruction, https://github.com/NNairIITK/Vreco_CPMD/tree/master (accessed: November 2024).
- [74] A. Savitzky, M. J. E. Golay, *Anal. Chem.* **1964**, *36*, 1627.
- [75] R. Resta, *Rev. Mod. Phys.* **1994**, *66*, 899.
- [76] N. Marzari, D. Vanderbilt, *Phys. Rev. B* **1997**, *56*, 12847.
- [77] N. Marzari, A. A. Mostofi, J. R. Yates, I. Souza, D. Vanderbilt, *Rev. Mod. Phys.* **2012**, *84*, 1419.
- [78] CPMD code, © 1990-2023 by IBM Corp. and © 1994-2001 by Max Planck Institute, Stuttgart, <https://github.com/CPMD-code> (accessed: November 2024).
- [79] J. Hutter, M. Iannuzzi, *Z. Kristallogr. - Cryst. Mater.* **2005**, *220*, 549.